This is a repository copy of *Vascular tree tracking and bifurcation points detection in retinal images using a hierarchical probabilistic model*.

Vascular Tree Tracking and Bifurcation Points Detection in Retinal Images Using a Hierarchical Probabilistic Model

Soodeh Kalaie[1]* , Ali Gooya[2]

[1]*Department of Electrical and Computer Engineering, Tarbiat Modares University, Tehran, Iran*
[2]*Department of Electronic and Electrical Engineering, University of Sheffield, Sheffield, UK*
[1]*s.kalaie@modares.ac.ir*

Abstract

Background and Objective: Retinal vascular tree extraction plays an important role in computer-aided diagnosis and surgical operations. Junction point detection and classification provide useful information about the structure of the vascular network, facilitating objective analysis of retinal diseases.
Methods: In this study, we present a new machine learning algorithm for joint classification and tracking of retinal blood vessels. Our method is based on a hierarchical probabilistic framework, where the local intensity cross sections are classified as either junction or vessel points. Gaussian basis functions are used for intensity interpolation, and the corresponding linear coefficients are assumed to be samples from class-specific Gamma distributions. Hence, a directed Probabilistic Graphical Model (PGM) is proposed and the hyperparameters are estimated using a Maximum Likelihood (ML) solution based on Laplace approximation.
Results: The performance of proposed method is evaluated using precision and recall rates on the REVIEW database. Our experiments show the proposed approach reaches promising results in bifurcation point detection and classification, achieving 88.67% precision and 88.67% recall rates.
Conclusions: This technique results in a classifier with high precision and recall when comparing it with Xu's method.

Keywords: Bifurcation, Classification, Machine learning, Probabilistic Graphical Model, Retinal blood vessel tracking.

1 Introduction

Retina is one of the most important organs in eye and acts as a detector for the incident light, enabling human vision. It consists of unique types of cells that are referred as sensory receptors. The retinal blood vessel network provides nutrition to eyes and removes waste from the retinal systems. Several retinal implications have been related to vascular anomalies and structural changes, which includes diabetic retinopathy, glaucoma, retinal artery occlusion and macular degeneration [1, 2]. In the field of medical diagnosis and surgical planning, vascular reconstruction and bifurcation detection in retinal images are basic steps for computerized analysis. Vascular bifurcation and branching in retinal images usually helps predicting diseases [3, 4]. Additionally, changes in the retinal vascular can be observed by the modification of bifurcation patterns.

Generally speaking, blood vessel segmentation methods can be divided into two main categories: pixel-based classification approaches, and center line tracking methods [5]. In the former group, pixels are represented by their corresponding feature vectors representing local properties, e.g. intensity and its higher order of derivatives. Next, these vectors are either classified using a ground truth data in a supervised fashion, or clustered through an unsupervised mechanism into homogeneous sets of vessel/non-vessel pixels. A complete review of these methods can be found in [5] and is beyond the scope of this paper. To outline our contributions in the proper context, each category is briefly discussed through a few exemplary methods.

Several supervised methods are introduced in [6, 7], where artificial neural networks have been explored for segmenting vascular features and making classification. Marin et al. [7] presented a neural network scheme for pixel classification. This methodology uses a 7-D feature vector composed of gray-level and moment invariants-based features for pixel representation. Similarly, Franklin et al. [8] presented a multilayer perceptron neural network, for which the inputs are derived from the Gabor and moment invariants-based features computed from the images. A supervised segmentation technique based on the deep neural networks is proposed in [9], where the neural network is trained on the large sample of database. Then the structure prediction network is used to classify multiple pixels. Fu et al. [10] utilized the convolutional neural network (CNN) combined with Conditional Random Field (CRF) to model long-range pixel interactions. Ricci et al. [11] proposed using line detection operators to compute feature vectors and Support Vector Machines (SVM) for pixel classification. Also, You et al. [12] exploited the radial projection and semi-supervised classification using SVM for vessel segmentation. A supervised method for retinal blood vessel segmentation is presented in [13]. They designed the feature vectors by combining local area and shape information with the multi-scale statistical features based on gray level values. Finally a support vector classifier is used for classification of pixels belonging to vasculatures. The application of a 2-D Gabor filter and Gaussian mixture model classifier has been demonstrated by Soares et al. [14]. Osareh et al. [15] proposed an automatic retinal blood vessel

segmentation technique, where a feature vector is computed using properties of scale and orientation selective Gabor filters. The extracted features are then classified using the Gaussian mixture model and SVM classifiers.

Similarly, various unsupervised pixel labeling approaches have been proposed. Segmentation of retinal blood vessels by combining a Difference of Offset Gaussian (DoOG) filter and morphological reconstruction is described in [16]. Kande et al. in [17] proposed an unsupervised fuzzy clustering algorithm which uses matched filtering to enhance vessels and background. An MRA fuzzy c-Means vessel segmentation algorithm based on the vascular feature, presented by Yang et al. [18], where the combination of both the tubular structural information and gray value scale information are utilized to segment cerebral vessels. The template matching is also a pixel based method which is an unsupervised technique. Matching filter based detection has been suggested to detect piecewise linear segments of blood vessels in [19–23]. For instance, Chaudhuri et al. use a two-dimensional linear kernel with a Gaussian profile to search for vessel segments along twelve directions [23]. Hoover et al. [24] benefit from combination of local and regional properties of retinal blood vessels for segmentation. They use a threshold probing technique on a matched filter response image.

Although pixel based approaches have been significantly developed due to their ease of implementation, they do not guarantee connectedness in the segmented structures, and hence topologically correct vessels. Tracking based methods, on the other hand, generate connected vessel centerlines and provide structural information describing the bifurcation points and the branches, which can be useful for compositional analysis of the vascular trees.

Vessel tracking algorithms start from seed points on the vessels, placed either automatically or manually, and follow centerlines using local structural information [25, 26]. These techniques usually find the path that best matches a vessel profile model. An adaptive tracking algorithm is described in [27], which identifies the incremental size of progression by exploiting the spatial continuity of the vessels centerline and orientation, ignoring bifurcations. Zhou at al. [28] developed an algorithm for quantification of centerline, diameter and tortuosity of a vessel segments. In this technique, a matched filter is combined with a prior knowledge to automatically detect edges and track the centerline. To model vessel intensity profiles. Gaussian functions were used that are not always realistic approximations.

The fuzzy c-mean clustering algorithm employed in [19] automatically track fundus vessels using linguistic descriptions like vessel and non-vessel. This iterative fuzzy vessel tracking algorithm is based on finding the membership functions of the two linguistic values. The method does not rely on edge information to locate the exact location of the vessels, which reduces the effects of noise in the tracking process. In the other technique, the use of Gaussian and Kalman filter for retinal blood vessel detection and tracking has been demonstrated by Chutatape et al. [26].

The multiscale second order derivatives of an image (Hessian) is examined by [29] with the context of developing a vessel enhancement filter. The eigenvalue analysis of the Hessian is used to find out the direction of least intensity variations and, hence, the local vessel orientation. Aylward et al. [30] successfully applied this information for centerline extraction and showed the robustness to presence of bifurcations but did not explicitly detect them. An improved vessel centerline tracking method is described by Xu et al. [31] that combines the recursive geometrical tracking method of Sun et al.'s algorithm [27] and the eigenvector of the Hessian used in Aylward et al.'s approach [30].

Delibasis et al. [32] have proposed an automatic model based tracking algorithm, which also estimates the diameter of the vessels. The algorithm utilizes a parametric model of a vessel and a measure of match (MoM) that quantifies the similarity between the model and the given angiographic image path. The initialization of seed pixels for vessel tracking is also done according to Frangi's vesselness filter [29]. Generally speaking, these model based approaches perform reasonably well in tracking centerlines of linear vessel segments but do not generalize well in handling complex bifurcation patterns.

Nayebifar et al. [33] presented a vessel tracking approach based on particle filtering. This method does not perform any patch based processing to extract the vessels based on some prior geometric model. Instead, the particle filter uses a probability density function (PDF) to describe the blood vessels. The product of the green and blue channels of the RGB retinal images is considered as a PDF for tracking procedure. Also, the Bayesian theory has been employed in vessel tracking [34–36]. To detect and track vessels, these methods consider a prior probability, which depends on the number of large intensity transitions on a semi-circular cross section.

In addition to vessels, detection of bifurcations have been investigated by a series of researchers. An automatic detection and classification of retinal vessel tree bifurcations and crossovers is proposed in [37]. In this method, morphological filters are utilized for detection. In [38] the geometrical properties are used to detect tree landmarks, which are then classified as bifurcations, branches and cross overs. Baboiu et al. [39] proposed a bifurcation detection method that is based on the scale space behavior of those structures. An analytical model for the bifurcation evolution with increasing scale is combined with eigenvalue analysis to create a bifurcationness filter. The COSFIRE (Combination Of Shifted FIlter REsponses) filter is presented for the detection of bifurcations in segmented retinal images [40]. COSFIRE filters are trainable keypoint detection operators, which are selective for a number of prototype bifurcations. In summary, the majority of the existing attempts do not jointly detect the bifurcations and extract the centerlines at the same time. Therefore, a full description for the geometry of the branches and the locations of the bifurcations often remains missing.

In this paper, a new vessel tracking approach is proposed that can provide joint descriptions of the centerlines and the branching points. We demonstrate a machine learning algorithm, based on a hierarchical probabilistic framework,

to detect and classify normal blood vessel and bifurcation points. Our paper presents a directed Probabilistic Graphical Model (PGM) where the hyperparameters are estimated using a Maximum Likelihood (ML) solution based on Laplace approximation.

The rest of the paper is organized as follows: Next section gives a general description and formulation of our method, including the concept of linear regression model and representations of probability distributions using probabilistic graphical models. Section 3 illustrates the analyses. Experimental results and the discussion are given in sections 4 and 5, respectively. Eventually, we conclude the paper in section 6.

2 Proposed vessel extraction method

Our algorithm is an iterative process consisting of two major steps: tracking and classification. At each tracking step, the cross-sectional vessel profile is regressed using a linear model. It's then classified using the proposed graphical model. In this paper, two types of vessel structure are considered: normal and bifurcation points, which are illustrated in Fig. 1a. As seen, in a normal point, only one vessel exists in the search window, whereas in a bifurcation point, a single vessel is divided into two branches in the searching region. Given that in retina images vessels are darker than background, the centerlines become intensity valleys. Therefore in general, the intensity profile with only one valley is often described as the normal point and the intensity profiles having two large valleys imply a bifurcation structure. However, to classify a tracking position, the proposed algorithm does not rely on counting these features. The method can be described as a joint regression classification approach, where the distribution of the intensity regression coefficients derives the classification. More intuitively, for a branching point, this distribution should allow for more incidence of large regression coefficients (of basis function). Whereas to regress a normal vessel structure, a fewer number of *active* basis functions, thus larger precision in their distribution, is required. The proposed PGM is a hierarchical implementation of these concepts as follows.

2.1 Model Structure

At the given step n a dynamic searching region is defined as an adaptive semi-circular cross section and vessel intensity profile can be extracted in searching window. This profile is expressed as observation data $\mathbf{t}_n$. In this model, $\mathbf{t}_n \in \mathbb{R}^L$ is defined as a vessel intensity profile and L is the number of sampling points on the semi-circular arc (see Fig. 1b). The proposed algorithm tends to regress and classify $\mathbf{t}_n$ as class variable $z_n \in \{0, 1\}$, where $z_n = 0$ and $z_n = 1$ represent the normal and bifurcation vessel respectively.

The goal of regression is to predict the values of vessel profiles vector $\mathbf{t}_n$. The target variable is expressed by vector $\mathbf{y}_n$ with additive white Gaussian noise, so that

$$\mathbf{t}_n = \mathbf{y}_n + \boldsymbol{\epsilon} \tag{1}$$
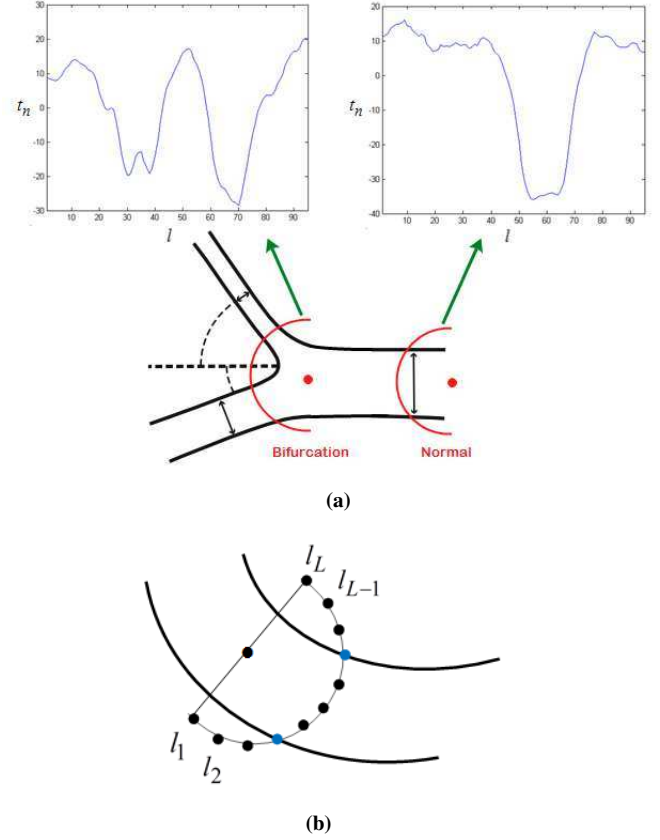

Fig. 1. Sectional intensity profile of a blood vessel: (a) Illustration of two types of blood vessel structures in the searching region (semi-circular arc); (b) Sampling points on the semi-circular arc.

where $\boldsymbol{\epsilon}$ is a zero mean normal distribution with precision β.

The simplest linear model for regression is one that involves a linear combination of the input variables. Thus the estimated vessel profile $\mathbf{y}_n$ is expressed as:

$$\mathbf{y}_n = \begin{pmatrix} y_{n1} \\ y_{n2} \\ \vdots \\ y_{nL} \end{pmatrix} = \begin{pmatrix} \boldsymbol{\phi}^T(l_1)\mathbf{w}_n \\ \boldsymbol{\phi}^T(l_2)\mathbf{w}_n \\ \vdots \\ \boldsymbol{\phi}^T(l_L)\mathbf{w}_n \end{pmatrix} = \begin{pmatrix} \boldsymbol{\phi}^T(l_1) \\ \boldsymbol{\phi}^T(l_2) \\ \vdots \\ \boldsymbol{\phi}^T(l_L) \end{pmatrix} \mathbf{w}_n \tag{2}$$

where $\boldsymbol{\phi}^T = (\phi_0, \phi_1, \ldots, \phi_{M-1})$ and $\phi(\cdot)$ are nonlinear functions of the input variables l_i and known basis functions. l_i is the length of the semi-circular arc corresponding to the i sampling point and $\mathbf{w}_n = (w_{n0}, w_{n1}, \ldots, w_{nM-1})^T$ are weighting variables. Linear combinations of these functions are supposed to extend the class of model. In this study, features can be expressed in term of basis functions and M denotes the number of features.

In the retinal images, vessel's sectional intensity profile can be approximated as a Gaussian curve [23]. We also use Gaussian basis functions, however because of regression, the profiles are not constrained to be Gaussian in this paper. Therefore, the basis functions utilized here is as following:

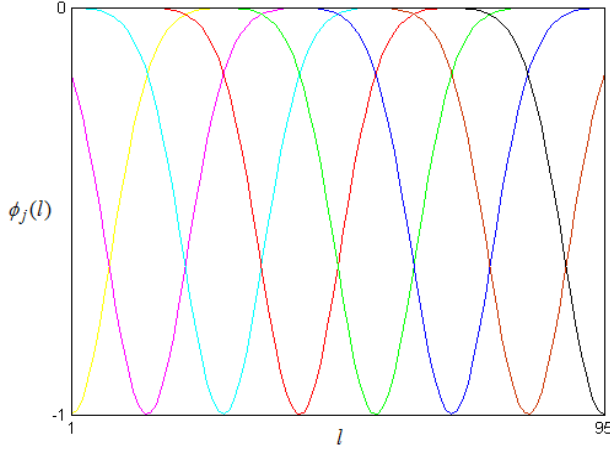$$\phi_j(l_i) = -exp\{-\frac{(l_i - \xi_j)^2}{2\sigma^2}\} \tag{3}$$

Fig. 2. Illustration of Gaussian basis functions for $M = 8$.

where the ξ_j for $j = (1, ..., M)$ denotes the location of basis functions in the input space, and the parameter σ controls the width of the functions (see Fig. 2).

Note that using (1), the conditional distribution of $\mathbf{t}_n$ given the weighting variables $\mathbf{w}_n$ is specified as:

$$p(\mathbf{t}_n|\mathbf{w}_n) = \mathcal{N}(\mathbf{t}_n|\mathbf{\Phi}\mathbf{w}_n, \beta^{-1}\mathbf{I}_{L \times L}) \qquad (4)$$

where according to (2), $\mathbf{\Phi}$ is an $L \times M$ design matrix, whose elements are defined by $\Phi_{ij} = \phi_j(l_i)$. Thus it is expressed by

$$\mathbf{\Phi} = \begin{pmatrix} \phi_0(l_1) & \phi_1(l_1) & \cdots & \phi_{M-1}(l_1) \\ \phi_0(l_2) & \phi_1(l_2) & \cdots & \phi_{M-1}(l_2) \\ \vdots & \vdots & \ddots & \vdots \\ \phi_0(l_L) & \phi_1(l_L) & \cdots & \phi_{M-1}(l_L) \end{pmatrix}. \qquad (5)$$

To construct a graphical representation of the data, we treat the weighting variables $\mathbf{w}_n$ as independent random samples from a Gaussian probability distribution, which is conjugate to the distribution given in (4). Hence, the probability of $\mathbf{w}_n$ is modelled as following:

$$p(\mathbf{w}_n|\mathbf{a}_n) = \prod_{m=0}^{M-1} p(w_{nm}|a_{nm}) \qquad (6)$$
$$= \prod_{m=0}^{M-1} \mathcal{N}(w_{nm}|0, a_{nm}^{-1})$$

where the vector $\mathbf{a}_n$ specifies the precision of the normal distribution. Finally, at the highest level, these precision variables are assumed to be random samples from class dependent Gamma distributions, conjugate to distributions

in (6). More specifically, we define

$$p(\mathbf{a}_n|z_n) = \left(\prod_{m=0}^{M-1} Gam(a_{nm}; k_0, \theta_0) \right)^{(1-z_n)} \qquad (7)$$
$$\times \left(\prod_{m=0}^{M-1} Gam(a_{nm}; k_1, \theta_1) \right)^{(z_n)}$$
$$= \prod_{m=0}^{M-1} \left(\frac{a_{nm}^{k_0-1}}{\Gamma(k_0)\theta_0^{k_0}} e^{-\frac{a_{nm}}{\theta_0}} \right)^{(1-z_n)}$$
$$\times \left(\frac{a_{nm}^{k_1-1}}{\Gamma(k_1)\theta_1^{k_1}} e^{-\frac{a_{nm}}{\theta_1}} \right)^{(z_n)}$$

where k_c, θ_c are class dependent shape and scale hyper parameters (c denotes the number of classes, e.g. vessel and bifurcation type).

2.2 Proposed PGM

Probabilistic graphical models are well used to describe machine learning and pattern recognition algorithms. In this study, a Bayesian network (directed graphical model) is proposed to illustrate causal relationships between variables (see Fig. 3a). We suppose data set of N observations $\{\mathbf{t}_n\}$ and $\{z_n\}$, where $n = 1, ..., N$, with corresponding latent variables $\{\mathbf{w}_n\}$ and $\{\mathbf{a}_n\}$. The actual observed data $\{\mathbf{t}_n\}$ and $\{z_n\}$ are known as incomplete data set. As shown in Fig. 3b, for N observation, $\theta = \{\theta_0, \theta_1\}$, β and $k = \{k_0, k_1\}$ are hyperparameters. We estimate the values of hyperparameters θ_0, θ_1 and β by maximizing the marginal likelihood function and manually set the values of k_0 and k_1 for simplicity.

The graphical representation leads to express the likelihood function simply by concept of i.i.d (independent identically distributed). The marginal likelihood function (or the evidence function) is evaluated in the next subsection.

2.3 Evidence Function

The marginal likelihood function (or model evidence) is obtained by integrating over vectors $\mathbf{w}_n$ and $\mathbf{a}_n$, so that

$$p(\mathbb{t}, \mathbb{z}|\theta, \beta) = \iint_{\mathbb{a}, \mathbb{w}} p(\mathbb{t}, \mathbb{z}, \mathbb{a}, \mathbb{w}|\theta, \beta) \, d\mathbb{a} \, d\mathbb{w} \qquad (8)$$
$$= \prod_{n=1}^{N} \iint_{\mathbf{a}_n, \mathbf{w}_n} p(\mathbf{t}_n, z_n, \mathbf{a}_n, \mathbf{w}_n|\theta, \beta) \, d\mathbf{a}_n \, d\mathbf{w}_n.$$

The marginalization with respect to $\mathbf{a}_n$ is as the follows:

$$\prod_{m=0}^{M-1} \int_{a_{nm}} p(w_{nm}|a_{nm}) \, p(a_{nm}|z_n) \, da_{nm} \qquad (9)$$
$$= \prod_{m=0}^{M-1} \frac{C(\theta_0, \theta_1, k_0, k_1, z_n)}{\sqrt{2\pi}}$$
$$\times \int_{a_{nm}} a_{nm}^{\left(\frac{1}{2} + (k_0-1)(1-z_n) + (k_1-1)z_n\right)}$$
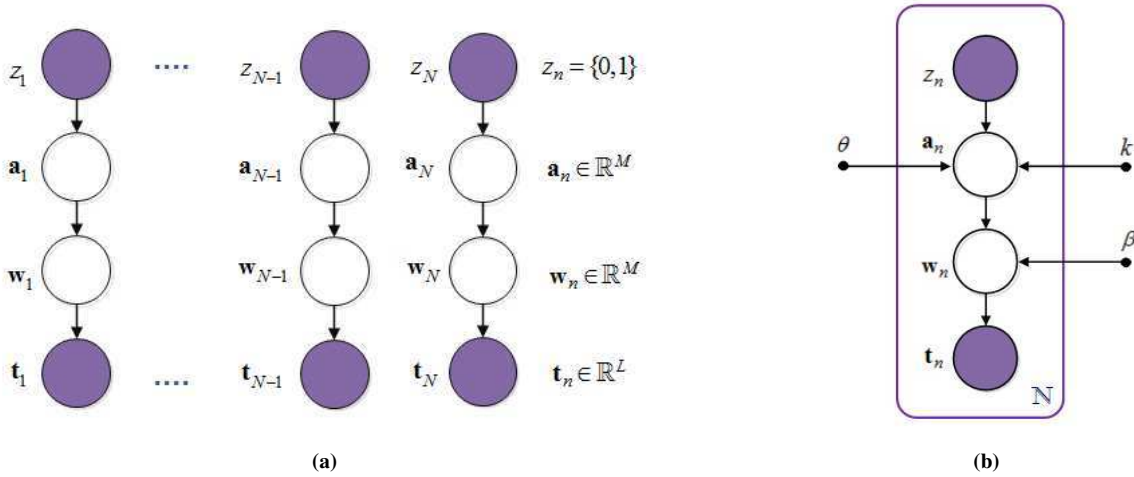$$\times e^{-a_{nm}\left(w_{nm}^2 + \frac{1-z_n}{\theta_0} + \frac{z_n}{\theta_1}\right)} \, da_{nm}$$

Fig. 3. (a) Proposed directed graphical model and (b) shows the same graph model as in (a) using the plate notation for $n = 1, ..., N$ observations.

where $C = \left(\left(\Gamma(k_0) \theta_0^{k_0} \right)^{(1-z_n)} \left(\Gamma(k_1) \theta_1^{k_1} \right)^{(z_n)} \right)^{-1}$. Since the probability density function is nonnegative everywhere and its integral over the entire space is equal to one, therefore we can use $\int_x Gam(x; a, b) \, dx = \int_x \frac{b^a}{\Gamma(a)} x^{a-1} e^{-bx} \, dx = 1$ to simplify the right-hand side of (9) as:

$$\prod_{m=0}^{M-1} \frac{C(\theta_0, \theta_1, k_0, k_1, z_n)}{\sqrt{2\pi}} \tag{10}$$

$$\times \Gamma\left(\frac{3}{2} + (k_0 - 1)(1 - z_n) + (k_1 - 1)z_n \right)$$

$$\times \left(w_{nm}^2 + \frac{1-z_n}{\theta_0} + \frac{z_n}{\theta_1} \right)^{-\left(\frac{3}{2} + (k_0-1)(1-z_n) + (k_1-1)z_n \right)}$$

The maximum likelihood solution for the hyperparameters has no closed-form analytical solution. Therefore, we evaluate the integral with respect to $\mathbf{w}_n$, using the Laplace approximation, which is based on a local Gaussian approximation centered on the mode of the function $f(w_{nm}) = \left(w_{nm}^2 + \frac{1-z_n}{\theta_0} + \frac{z_n}{\theta_1} \right)^{-\left(\frac{3}{2} + (k_0-1)(1-z_n) + (k_1-1)z_n \right)}$. This provides a practical alternative to the evidence framework. A Gaussian approximation of the function $f(w_{nm})$ can be expressed as (please refer to the Appendix section):

$$f(w_{nm}) \tag{11}$$
$$\simeq \left(\frac{1}{\theta} \right)^{-(k+\frac{1}{2})} \frac{\sqrt{2\pi}}{\sqrt{2\theta(k+\frac{1}{2})}} \mathcal{N}\left(w_{nm} | 0, \left(2\theta(k+\tfrac{1}{2}) \right)^{-1} \right).$$

Hence the Laplace method leads to a simple closed-form analytical solution for the hyperparameters. Therefore, the evidence function (8) can be simplified to (12).

$$p(\mathbb{t}, \mathbb{z} | \theta, \beta) = \prod_{n=1}^{N} (2k+1)^{-\frac{M}{2}} \left(\frac{\Gamma(k+0.5)}{\Gamma(k)} \right)^M \tag{12}$$

$$\times \int_{\mathbf{w}_n} \mathcal{N}(\mathbf{t}_n | \mathbf{\Phi} \mathbf{w}_n, \beta^{-1} \mathbf{I}_{L \times L}) \mathcal{N}\left(\mathbf{w}_n | 0, b_n^{-1} \mathbf{I}_{M \times M} \right) \, d\mathbf{w}_n$$

where M denotes the dimensionality of $\mathbf{w}_n$ and $b_n = 2(k+0.5)/(\frac{1-z_n}{\theta_0} + \frac{z_n}{\theta_1})$. The parameter b_n specifies the precision of distribution over $\mathbf{w}_n$ which consists of class variables z_n to classify the intensity profiles by the weighting variables $\mathbf{w}_n$.

To evaluate the integral in (12), we use the result of Bayes theorem for conditional distribution in a linear-Gaussian model. Also, we evaluate the integral by computing a quadratic form in the exponent and making use of it for the normalization coefficient of Gaussian. Therefore, the evidence function can be rewritten as:

$$p(\mathbb{t}, \mathbb{z} | \theta, \beta) = \prod_{n=1}^{N} (2k+1)^{-\frac{M}{2}} \left(\frac{\Gamma(k+0.5)}{\Gamma(k)} \right)^M \tag{13}$$

$$\times \left(\frac{\beta}{2\pi} \right)^{\frac{L}{2}} \left(\frac{b_n}{2\pi} \right)^{\frac{M}{2}} \int_{\mathbf{w}_n} \exp\left\{ -E(\mathbf{w}_n) \right\} \, d\mathbf{w}_n.$$

The total error function is given by

$$E(\mathbf{w}_n) = \frac{\beta}{2} \| \mathbf{t}_n - \mathbf{\Phi} \mathbf{w}_n \|^2 + \frac{b_n}{2} \mathbf{w}_n^T \mathbf{w}_n \tag{14}$$

where the term $\frac{b_n}{2}$ is considered to regulize the error function. It has the property that if b_n is sufficiently large; some of the components of $\mathbf{w}_n$ are driven to zero, leading to a sparse model in which the corresponding basis functions play no role. Also the value of hyperparameters θ_0 and θ_1 modify value of b_n in each class.

Using the result of Bayes theorem for conditional distribution, we have $p(\mathbf{w}_n | \mathbf{t}_n) = \mathcal{N}(\mathbf{w}_n | \boldsymbol{\mu}_n, \mathbf{A}_n^{-1})$. Where $\boldsymbol{\mu}_n = \beta \mathbf{A}_n^{-1} \mathbf{\Phi}^T \mathbf{t}_n$ and $\mathbf{A}_n = b_n \mathbf{I}_{M \times M} + \beta \mathbf{\Phi}^T \mathbf{\Phi}$. Therefore, square error over $\mathbf{w}_n$ can be expressed as:

$$E(\mathbf{w}_n) = E(\boldsymbol{\mu}_n) + \frac{1}{2} (\mathbf{w}_n - \boldsymbol{\mu}_n)^T \mathbf{A}_n (\mathbf{w}_n - \boldsymbol{\mu}_n) \tag{15}$$

where $\mathbf{A}_n$ corresponds to the Hessian matrix of the error function, and

$$E(\boldsymbol{\mu}_n) = \frac{\beta}{2} \| \mathbf{t}_n - \mathbf{\Phi} \boldsymbol{\mu}_n \|^2 + \frac{b_n}{2} \boldsymbol{\mu}_n^T \boldsymbol{\mu}_n. \tag{16}$$

Thus the maximum weight vector is expressed by $\mathbf{w}_n^* = \boldsymbol{\mu}_n$ and sectional intensity profiles are provided by $\mathbf{y}_n(\mathbf{l}, \mathbf{w}_n^*)$. The hyperparameters can be estimated by maximizing the logarithm of marginal likelihood in the next subsection.

2.4 Hyperparameter Estimation

In this section, the logarithm of evidence function is maximized with respect to hyperparameters θ and β. In the other word, the best hyperparameters are

$$\hat{\theta}, \hat{\beta} = \arg\max_{\theta,\beta}\{\ln p(\mathbb{t}, \mathbb{z}|\theta, \beta)\}. \tag{17}$$

The value of β that maximizes the marginal likelihood can be obtained as:

$$\frac{1}{\beta} = \frac{1}{NL - \sum\limits_{n=1}^{N}\rho_n}\sum_{n=1}^{N}\sum_{i=1}^{L}\big(t_{ni} - \boldsymbol{\mu}_n^T\phi(l_i)\big)^2. \tag{18}$$

where the quantity ρ_n can be written $\rho_n = \sum\limits_{i=1}^{M}(\nu_i/(\nu_i + b_n))$ and ν_i are the eigenvalues of $\beta\boldsymbol{\Phi}^T\boldsymbol{\Phi}$ matrix.

This shows that β is obtained using an implicit solution technique. Thus a chosen initial value of β can be used to calculate $\boldsymbol{\mu}_n$ and ρ_n and then re-estimate β by (18), repeating until convergence. Similarly, the values of θ can be determined using maximizing the logarithm of evidence function with respect to θ_0 and θ_1.

$$\theta_0 = \frac{MN_0}{2(k+0.5)\Big(\sum\limits_{n=1}^{N}\boldsymbol{\mu}_n^T\boldsymbol{\mu}_n + \sum\limits_{n=1}^{N}\sum\limits_{i=1}^{M}\frac{1}{\nu_i+b_n}\Big)}. \tag{19}$$

$$\theta_1 = \frac{MN_1}{2(k+0.5)\Big(\sum\limits_{n=1}^{N}\boldsymbol{\mu}_n^T\boldsymbol{\mu}_n + \sum\limits_{n=1}^{N}\sum\limits_{i=1}^{M}\frac{1}{\nu_i+b_n}\Big)}. \tag{20}$$

where $N = N_0 + N_1$, N_0 and N_1 represent the number of data belongs to normal vessels and bifurcation points, respectively.

Note that the presented equations are also implicit solutions for θ, because the parameter b_n and matrix $\boldsymbol{\mu}_n$ depend on θ. Thus, the solution is an iterative procedure in which an initial choice is made for θ and uses to determine $\boldsymbol{\mu}_n$, as well as b_n. These values are then used to re-estimate hyperparameters θ_0, θ_1 using (19) and (20).

3 Analysis

Fig. 4 shows the schematic diagram of our proposed approach for retinal vessel tracking. As a preprocessing step, we extract green channel from RGB image. This algorithm is performed on this particular channel, because this channel provides the highest contrast between the retinal vessels and background. The green channel usually has considerable image information while red channel is the brightest color channel and has low contrast, and the blue channel is rather dark and does not contain any information [41]. In the first stage, several vessel's intensity profiles are extracted from chosen section of image in two different classes.

These intensity profiles organize the training and test data for cross validation. Then the proposed machine learning process is used to estimate the model hyperparameters and predict the class of blood vessels. In this paper, leave-one-out cross validation is employed to estimate how accurate our predictive model performs in practice. On the other hand, the goal algorithm is to achieve accurate estimation $\mathbf{y}_n$ and the class label parameters consequently. Therefore, to determine the best value of M the square error value between the observed and predicted profiles, i.e. $\mathbf{t}_n$ and $\mathbf{y}_n$, can be evaluated for training and test data set. In the second stage, the following iterative process is used to describe the tracking and classification algorithm:

The tracking progress is similar to the method proposed in [34] but with difference that the cross-sectional vessel profile is regressed using a linear regression model at each tracking step and then classified by the proposed graphical model.

- *Initialization*: At first, two initial edge points are manually selected diametrically on the desired vessel, and the middle point of current edges is expressed as initial center point (see Fig. 5a).
- *Tracking*: At the current iteration, the intensity profile $\mathbf{t}_n$ is extracted in a semi-circular search window. Then this profile is estimated as $\mathbf{y}_n$ using the proposed linear regression mentioned in (2). Therefore, the ridge of estimated profile $\mathbf{y}_n$ is considered as the center point O_n. At step n, we define vessel edge points U_n, V_n, center point O_n, direction $\overrightarrow{D_n}$ and diameter d_n. The tracking direction $\overrightarrow{D_n}$ is $\overrightarrow{O_{n-1}O_n}$ and local vessel diameter is defined as $d_n = |\overrightarrow{U_nV_n}|$ (see Fig. 5b). The next vessel edge points are searched in a dynamic search window. These edges are identified by the defined threshold in [27].
  Using vessel diameter value resulted from previous step, a semi-circle can be adapted automatically with the radius of $1.2d_{n-1}$. Also the value of σ (mentioned in (3)) is upgraded by $\sigma = \frac{d_n}{4}$.
- *Classification*: During the tracking, vessel structure should be identified automatically. According to obtained hyperparameters, semi-circular intensity profiles are classified by predictive distribution, which is defined as follows:

$$p(z_n|\mathbf{t}_n, \mathbb{t}, \mathbb{z}, \theta, \beta) \tag{21}$$
$$= \iint\limits_{\mathbf{a}_n,\mathbf{w}_n} p(z_n|\mathbf{t}_n, \mathbf{w}_n, \mathbf{a}_n, \mathbb{t}, \mathbb{z}, \theta_0, \theta_1, \beta)$$
$$\times p(\mathbf{w}_n|\mathbf{a}_n)p(\mathbf{a}_n|z_n), d\mathbf{a}_n\,d\mathbf{w}_n$$
$$\propto \iint\limits_{\mathbf{a}_n,\mathbf{w}_n} p(z_n)p(\mathbf{t}_n|z_n, \mathbf{w}_n)p(\mathbf{w}_n|\mathbf{a}_n)p(\mathbf{a}_n|z_n)\,d\mathbf{a}_n\,d\mathbf{w}_n$$

The prior probability has the expression

$$p(z_n) = \Big(\frac{N_0}{N}\Big)^{(1-z_n)}\Big(\frac{N_1}{N}\Big)^{(z_n)} \tag{22}$$

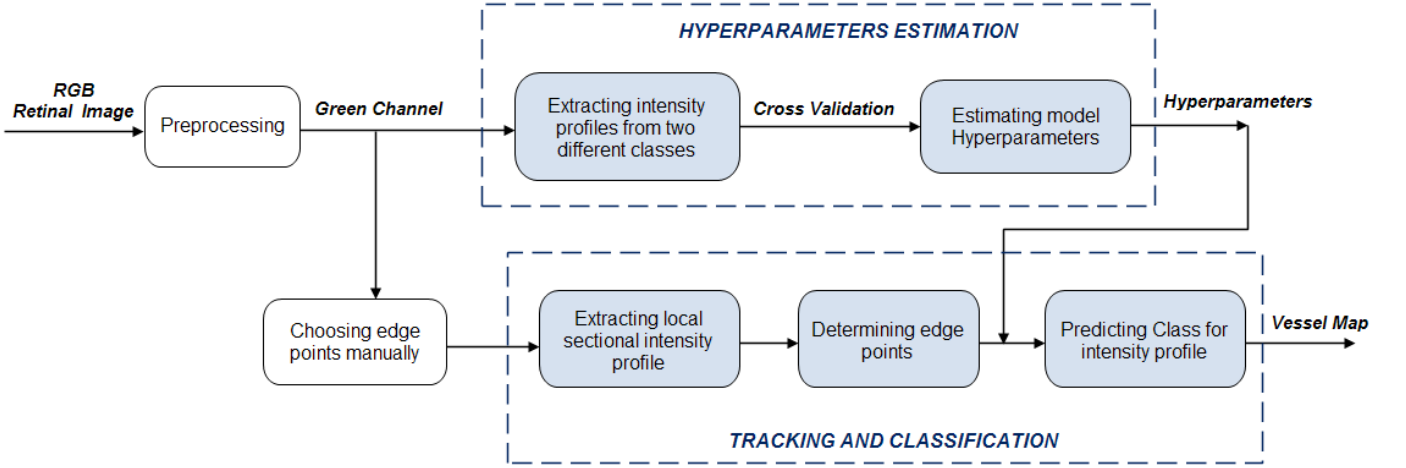which is weighted by the number of training data belonging to normal and bifurcation structures. Using (12) and

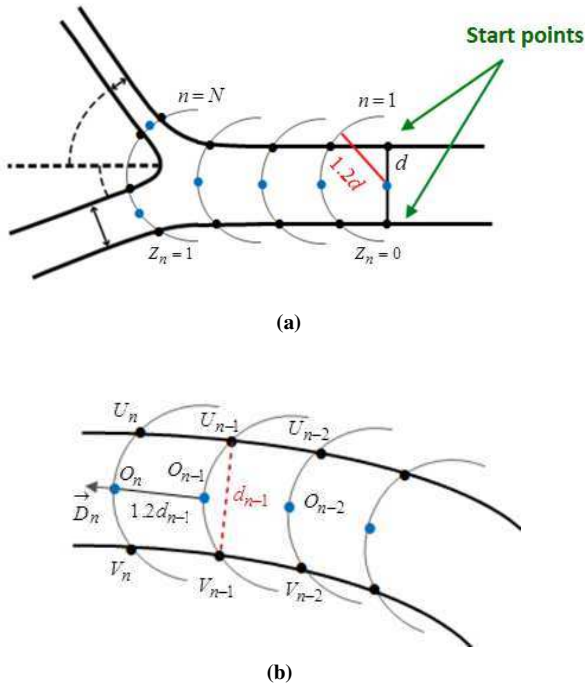Fig. 4. Schematic diagram of the proposed method.

(a)

(b)

Fig. 5. Definition of dynamic searching region and tracking process.

the result of Bayes theorem, predictive distribution can be simplified into the following

$$p(z_n|\mathbf{t}_n, \mathbb{t}, \mathbb{z}, \theta, \beta) = \left(\frac{N_0}{N}\right)^{(1-z_n)}\left(\frac{N_1}{N}\right)^{(z_n)} \quad (23)$$

$$\times (2k+1)^{-\frac{M}{2}}\left(\frac{\Gamma(k+0.5)}{\Gamma(k)}\right)^M$$

$$\times \mathcal{N}(\mathbf{t}_n|0, \beta^{-1}\mathbf{I}_{L\times L} + \mathbf{\Phi}b_n^{-1}\mathbf{I}_{M\times M}\mathbf{\Phi}^T).$$

It should be noted that the proposed tracking method is reasonably robust to a non-optimal initial point selection. The tracking based methods usually require the user to define the initial points. In our method two diametrical initial points are used to define the radius of semi-circle arc in the first step. Therefore non-optimal selection for

one point only leads to an increase in d and the radius of the first semi-circular window consequently. At the next step the proposed algorithm automatically modifies diameter using the threshold resulted from the previous semi-circular window.

In general, this tracking process automatically stops when the vessel diameter is less than five pixels. Besides, where the bifurcation points are found the tracking method continues in larger branch and the other one is tracked subsequently.

4 Experimental results

To evaluate the performance of our proposed method, the retinal images from the REVIEW [42] and DRIVE [43] databases are used to assess the performance of vessel classification algorithm. The REVIEW database consists of four datasets HRIS, VDIS, CLRIS and KPIS, including 16 images with 193 vessel segments, demonstrating a variety of pathologies and vessel types. Images are assessed by three independent experts, who marked the vessel edges. Also, the DRIVE database consists of 89 color fundus images of which 84 contain signs of the diabetic retinopathy and 5 are considered as healthy.

We evaluate the accuracy of both bifurcation and normal points, in the manually graded images by an expert compared to the output images produced by our method. Since vessel crossing configuration is not considered in the proposed model, the proposed algorithm is applied to regions without significant crossing patterns.

Some examples of vessel tracking and classification in HRIS database are shown in Fig. 6. The first and second rows show healthy and disease subimages respectively, in which the disease images include retinal pathologies. Fig. 7 shows the experimental results of our algorithm in DRIVE database. The corresponding results using our tracking and classification method are shown on the green channel. These results are obtained by stopping the proposed tracking process manually. The cross sectional intensity profiles are classified as bifurcation points, shown by 1 (purple) and the normal vessels determined by 0 (green).
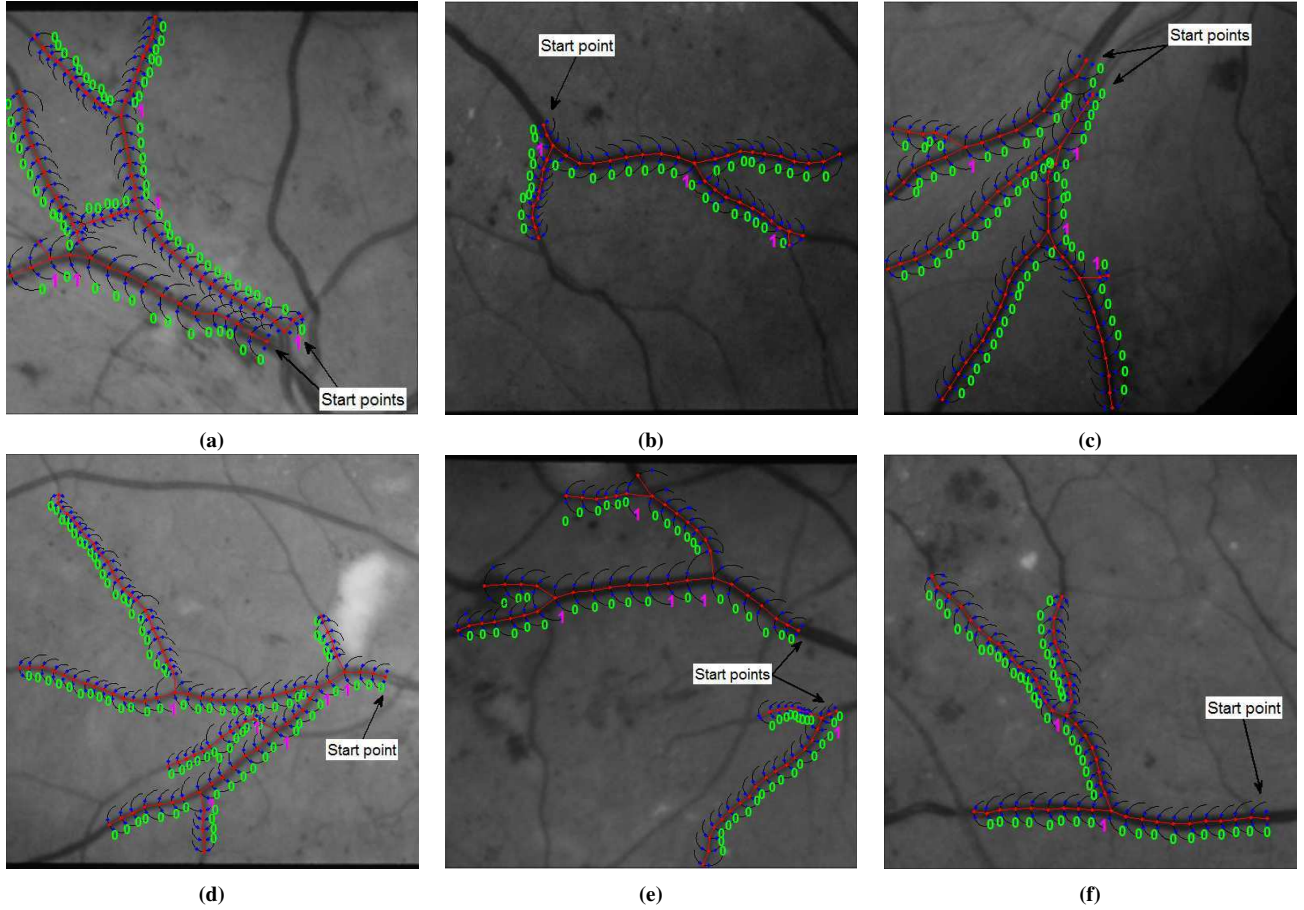
Fig. 6. Examples of vessel tracking and classification in the HRIS database: (a)-(c) and (d)-(f) present the results of proposed method on the healthy and disease images respectively.

In this paper, the Gaussian model has been proposed which fits the intensity profile of a retinal vessel. Hence, in some cases where the central vessel reflex, retinal pathologies or hardly noise are presented, the profile model can further complicate and misjudgment occurs in class detection (see Fig. 6e).

As previously mentioned in section 3, to determine the best value of M the residual value of $E(\mathbf{w}_n^*)$ mentioned in (16), can be evaluated for training and test data set. It is more convenient to use the root-mean-square (RMS) error defined by

$$E_{RMS} = \sqrt{2E(\mathbf{w}_n^*)/L} \qquad (24)$$

Fig. 8 shows the RMS error, evaluated on the training set and an independent test set for various values of M. The residual data error is reduced from $M = 8$ and $M = 9$. The generalization error is roughly constant between $M = 10$ and $M = 20$. However, $M = 10$ is simplest model which gives a good description for the observed data.

Fig. 9a shows the real and regressed intensity profile from the normal blood vessel. The coefficient parameters $\mathbf{w}_n^*$ is proportional to normal structure (see Fig. 9b). The bifurcation structure is shown in Fig. 9c and Fig. 9d which two elements of parameters $\mathbf{w}_n^*$ are larger than the other, thus the corresponding Gaussian basis functions is more effective to estimate bifurcation intensity profile.

5 Discussion

In the proposed classification model, any vessel section is classified either as normal vessel or junction points. Consequently, there are four events, where TP (true positives) represents the number of true bifurcation points detected; FP (false positives) is the number of falsely detected Bifurcation points; TN (true negatives) indicates the number of correctly detected normal vessels and FN (false negatives) is the number of falsely detected normal vessels.

Hence, for evaluation of the proposed classification algorithm, we introduce two criteria: the precision and recall of class prediction. They are defined as follows:

$$Precision = \frac{TP}{TP + FP} \qquad (25)$$

$$Recall = \frac{TP}{TP + FN} \qquad (26)$$

Table I shows these criteria with various number of basis function in N data set, with the best results achieved in $M = 10$. It confirm the results of RMS error evaluation.

To analysis bifurcation point detection, we use the criteria defined in (25) and (26). Table II shows the precision and recall rates resulted from the proposed method and Xu et al.'s method [31] on REVIEW database.

In this section, we compare our method to Xu et al.'s method proposed in [31]. In contrary to our method, they
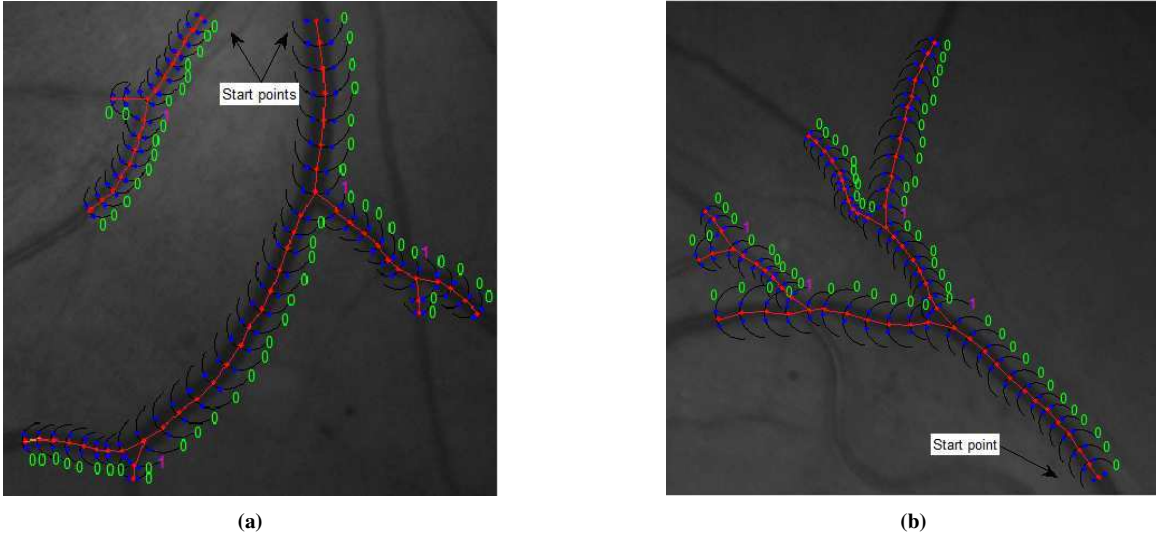
(a)

(b)

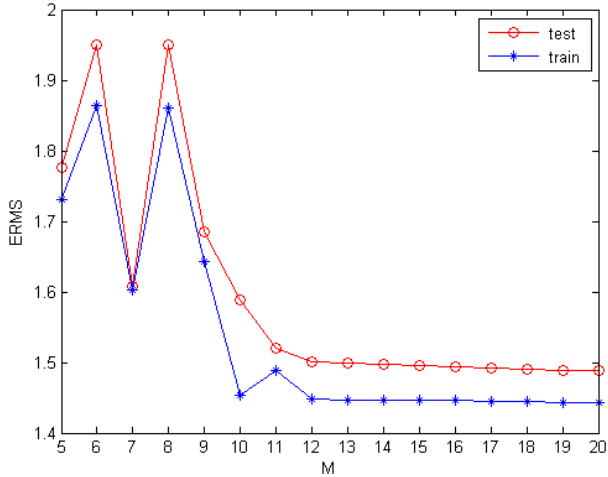Fig. 7. Examples of vessel tracking and classification in the DRIVE database.

Fig. 8. Graphs of the root-mean-square error, evaluated on the training set and on an independent test set for various values of M.

TABLE I.
Results for bifurcation classification with various number of basis functions.

M	8	9	**10**	11	12	13	14	15
Recall %	60.0	60.0	**83.3**	80.0	50.0	60.0	66.6	66.6
Precision %	50.0	37.5	**78.1**	57.1	50.0	50.0	57.1	57.1

directly use the intensity features obtained from the cross sections as follows: Inferring the directions of the vessels using a combination of approaches outlined in [27] and [30], the intensity profiles on the cross sections are convolved with a matched filter. The expected pattern for vessel cross-sectional intensity profile is assumed to be a rectangular in shape with width equal to 2R+1. These widths are then classified as either normal vessel or bifurcation points using a heuristic rule.

Table II summaries our comparisons showing that the

TABLE II.
Evaluation of bifurcation points detected on REVIEW database.

		Total	Healthy	Disease[*]
Proposed method	**Recall**%	**88.67**	**100.00**	**83.78**
	Precision%	**88.67**	**94.11**	**86.11**
Xu et al.'s method [31]	**Recall**%	64.15	77.77	57.14
	Precision%	66.66	70.00	64.51

[*]Images contain retinal pathologies.

proposed method is more precise than Xu et al.'s method [31]. This can be due to the fact that the classification rules in [31] are only heuristic and thus not always optimal.

In general, detected results in table II show that precision and recall rates have the same values for the proposed algorithm. It can be concluded from (25) and (26) that $FP = FN$. This demonstrates our model can recognize number of bifurcation branches successfully. In the healthy images, all bifurcation points are identified and only in few cases (5.89%) extra bifurcation structure are detected. In the disease cases, the model was successful in identifying the majority of the bifurcation points (83.78%) and in the 13.89% of cases determined false bifurcations.

Table III, shows the three criterions to compare the performance of the proposed method: TPR (recall), TNR and Accuracy (Acc) on the REVIEW and DRIVE databases. These metrics are defined as

$$TNR = \frac{TN}{TN + FP} = 1 - FPR \tag{27}$$

$$Accuracy = \frac{TP + TN}{TP + TN + FP + FN} \tag{28}$$

TPR measures the rate of real junction points correctly classified while TNR measures the rate of real normal vessels versus all the points classified as a normal vessel.
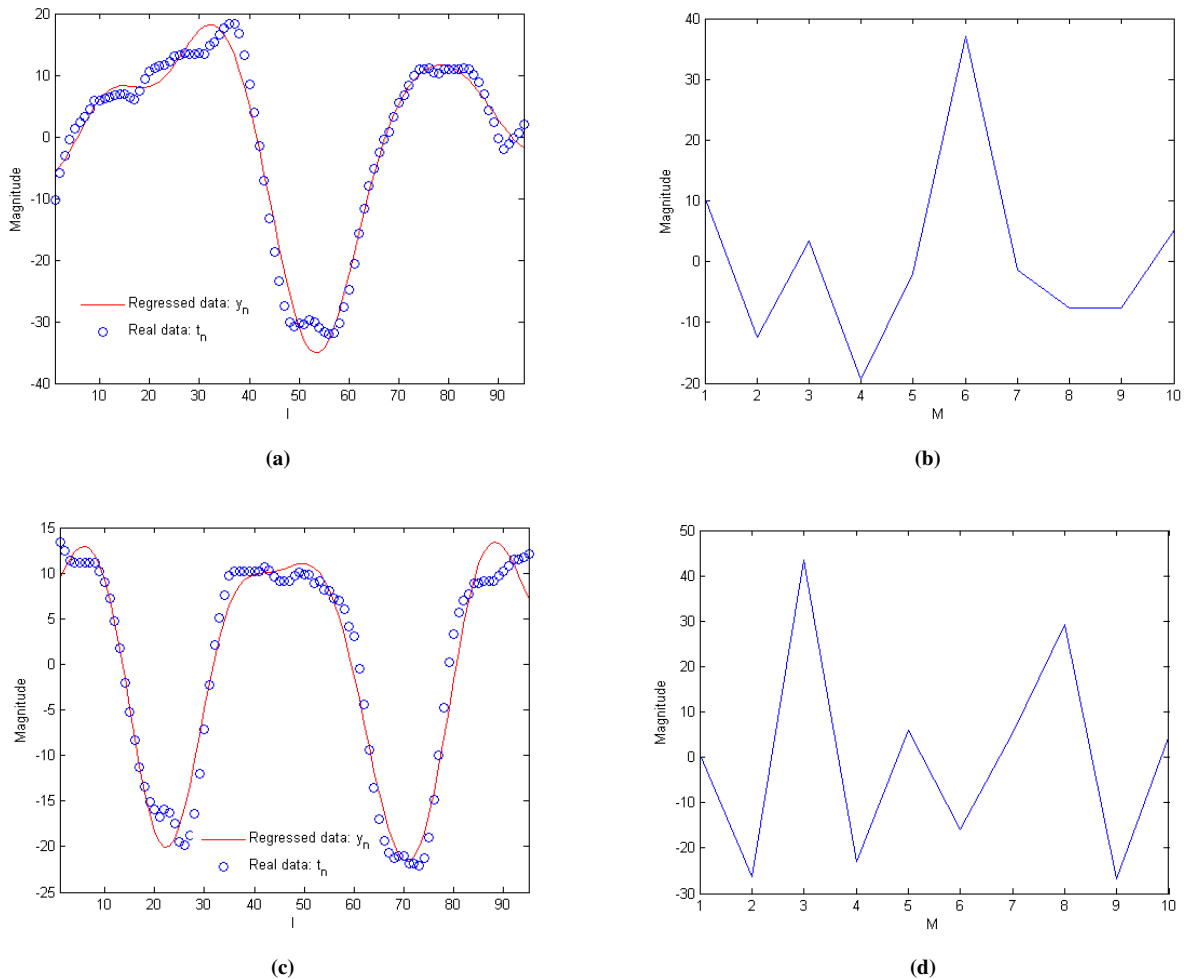
Fig. 9. (a) The real and regressed cross-sectional intensity profile of the normal structure. (b) Coefficient parameter ($\mathbf{w}_n^*$) distribution belongs to the normal structure. (d) The real and regressed cross-sectional intensity profile of the bifurcation structure. (d) Coefficient parameter ($\mathbf{w}_n^*$) distribution belongs to the bifurcation configuration.

TABLE III.
Comparison of different methods for retinal vessel classification on the REVIEW and DRIVE databases.

		Acc	TPR	1-FPR=TNR
REVIEW	Proposed method	**0.984**	**0.886**	**0.991**
	Xu et al.'s method [31]	0.952	0.641	0.975
DRIVE	Proposed method	**0.970**	**0.796**	**0.989**
	Xu et al.'s method [31]	0.968	0.666	0.968

In general, our method obtains better Acc score in the vessel classification and the main improvement comes in the TPR rate, due to the presented method do not use the intensity features for classification. It automatically reduces the dimensionality of the feature space and removes the noise before classification, due to its hierarchical structure. Also, the proposed method is more successful in the REVIEW database, because this database contains higher resolution images.

In this paper, all implementation have been done using MATLAB, on a Corei7 2.10 GHz Laptop PC running Windows 7 OS. The average processing time for the proposed algorithm (Edge detection, centerline detection and classification) on an image (720×715) was 28.1 s. The average processing time for Xu et al.'s method [31] (centerline detection and classification) on the same image was 27.7 s.

6 Conclusion

In this paper, we proposed a new vessel tracking method that is able to classify vessels as either normal vessel or bifurcation points. The retinal vascular tree is detected using vessel information and classification of the detected points conducted subsequently. The superiority of our tracking method over previous researches is to describe centerline and the bifurcation points simultaneously. We demonstrate a new machine learning algorithm, based on hierarchical probabilistic framework to detect and classify cross sectional intensity profiles. Gaussian basis functions are proposed to interpolate intensity profiles and the corresponding linear

coefficients are considered to be samples from class-specific Gamma distributions. Therefore, we presented a directed probabilistic graphical model where the hyperparameters are estimated using a maximum likelihood solution based on Laplace approximation.

The advantages of the proposed method is that it can estimate model hyperparameters without tuning these. Also, we did not use the intensity features for classification because these features can often contain noisy information lowering the training quality. Our method automatically reduces the dimensionality of the feature space and removes the noise before classification, due to its hierarchical structure.

In the proposed algorithm, the edge detection process is only an auxiliary method to update the radius of semi-circle window based on vessel diameter. Thus, vessel centerlines detection are obtained by using the regressed intensity profile.

In general, we provided a tree map of normal vessel and junction points on the vascular network, which can be used in diagnosis of cardiovascular diseases, image registration, biometrics or surgical applications. This novel algorithm is applied on the retinal images from the REVIEW and DRIVE databases. This technique results in a classifier with high accuracy, precision and recall. In future, we will extend the proposed framework to detect vessel crossings, in addition to bifurcation points considered in this paper.

Appendix A
Laplace Approximation

The Laplace method is utilized to find a Gaussian approximation $q(x)$ that is located on a mode of the function $f(x)$. Point x_0 is the mode of $f(x)$. We consider a Taylor's series expansion of $\ln f(x)$ around the peak x_0 :

$$\ln f(x) \simeq \ln f(x_0) - \frac{1}{2}A(x - x_0)$$

where

$$A = -\frac{d^2}{dx^2}\ln f(x)|_{x=x_0}$$

We then approximate $f(x)$ by an unnormalized Gaussian

$$f(x) \simeq f(x_0)\exp\{-\frac{A}{2}(x - x_0)^2\}$$

When the precision A is nonnegative, the Gaussian approximation could be well defined. That means the point x_0 be required to a local maximum. Hence, the second derivative of $f(x)$ at the stationary point x_0 is negative.

Here, we have

$$f(w_{nm}) = \begin{cases} \left(w_{nm}^2 + \frac{1}{\theta_0}\right)^{-\left(k_0 + \frac{1}{2}\right)} & \text{if } z_n = 0, \\ \left(w_{nm}^2 + \frac{1}{\theta_1}\right)^{-\left(k_1 + \frac{1}{2}\right)} & \text{if } z_n = 1. \end{cases}$$

The stationary point found as $w_0 = 0$, then the Hessian matrix at this mode expressed as follows:

$$A = -\frac{d^2}{dw^2}\ln f(w)|_{w=0} = 2\theta\left(k + \frac{1}{2}\right)$$

Therefore, $f(w_{nm})$ can be express as:

$$f(w_{nm}) \simeq \left(\frac{1}{\theta}\right)^{-\left(k + \frac{1}{2}\right)}\exp\{-\theta\left(k + \frac{1}{2}\right)w_{nm}^2\}$$

and

$$2\theta\left(k + \frac{1}{2}\right) > 0 \implies k > -\frac{1}{2}$$

References

[1] A. Alm, Ocular circulation, Adler's Physiology of the Eye.

[2] J. P. Gieser, M. Mori, N. P. Blair, M. Shahidi, Findings on retinal topography and thickness mapping in age-related macular degeneration, Retina 21 (4) (2001) 352–360.

[3] B. Wasan, A. Cerutti, S. Ford, R. Marsh, Vascular network changes in the retina with age and hypertension., Journal of hypertension 13 (12) (1995) 1724–1728.

[4] T. Teng, M. Lefley, D. Claremont, Progress towards automated diabetic ocular screening: a review of image analysis and intelligent systems for diabetic retinopathy, Medical and Biological Engineering and Computing 40 (1) (2002) 2–13.

[5] M. M. Fraz, P. Remagnino, A. Hoppe, B. Uyyanonvara, A. R. Rudnicka, C. G. Owen, S. A. Barman, Blood vessel segmentation methodologies in retinal images–a survey, Computer methods and programs in biomedicine 108 (1) (2012) 407–433.

[6] R. Nekovei, Y. Sun, Back-propagation network and its configuration for blood vessel detection in angiograms, IEEE Transactions on Neural Networks 6 (1) (1995) 64–72.

[7] D. Marín, A. Aquino, M. E. Gegúndez-Arias, J. M. Bravo, A new supervised method for blood vessel segmentation in retinal images by using gray-level and moment invariants-based features, Medical Imaging, IEEE Transactions on 30 (1) (2011) 146–158.

[8] S. W. Franklin, S. E. Rajan, Retinal vessel segmentation employing ann technique by gabor and moment invariants-based features, Applied Soft Computing 22 (2014) 94–100.

[9] P. Liskowski, K. Krawiec, Segmenting retinal blood vessels with deep neural networks, IEEE transactions on medical imaging 35 (11) (2016) 2369–2380.

[10] H. Fu, Y. Xu, D. W. K. Wong, J. Liu, Retinal vessel segmentation via deep learning network and fully-connected conditional random fields, in: Biomedical Imaging (ISBI), 2016 IEEE 13th International Symposium on, IEEE, 2016, pp. 698–701.

[11] E. Ricci, R. Perfetti, Retinal blood vessel segmentation using line operators and support vector classification, Medical Imaging, IEEE Transactions on 26 (10) (2007) 1357–1365.

[12] X. You, Q. Peng, Y. Yuan, Y.-m. Cheung, J. Lei, Segmentation of retinal blood vessels using the radial projection and semi-supervised approach, Pattern Recognition 44 (10) (2011) 2314–2324.

[13] Z. Han, Y. Yin, X. Meng, G. Yang, X. Yan, Blood vessel segmentation in pathological retinal image, in: Data Mining Workshop (ICDMW), 2014 IEEE International Conference on, IEEE, 2014, pp. 960–967.

[14] J. V. Soares, J. J. Leandro, R. M. Cesar Jr, H. F. Jelinek, M. J. Cree, Retinal vessel segmentation using the 2-d gabor wavelet and supervised classification, Medical Imaging, IEEE Transactions on 25 (9) (2006) 1214–1222.

[15] A. Osareh, B. Shadgar, Automatic blood vessel segmentation in color images of retina, Iran. J. Sci. Technol. Trans. B: Engineering 33 (B2) (2009) 191–206.

[16] A. M. Mendonca, A. Campilho, Segmentation of retinal blood vessels by combining the detection of centerlines and morphological reconstruction, Medical Imaging, IEEE Transactions on 25 (9) (2006) 1200–1213.

[17] G. B. Kande, P. V. Subbaiah, T. S. Savithri, Unsupervised fuzzy based vessel segmentation in pathological digital fundus images, Journal of medical systems 34 (5) (2010) 849–858.

[18] J. Yang, S. Ma, W. Tan, Q. Sun, P. P Cao, D. Zhao, Mra fuzzy c-means vessel segmentation algorithm based on tubular structure, Journal of Medical Imaging and Health Informatics 5 (8) (2015) 1853–1858.

[19] Y. Tolias, S. M. Panas, et al., A fuzzy vessel tracking algorithm for retinal images based on fuzzy clustering, Medical Imaging, IEEE Transactions on 17 (2) (1998) 263–273.

[20] X. W. Gao, A. Bharath, A. Stanton, A. Hughes, N. Chapman, S. Thom, Quantification and characterisation of arteries in retinal images, Computer methods and programs in biomedicine 63 (2) (2000) 133–146.

[21] L. Zhang, Q. Li, J. You, D. Zhang, A modified matched filter with double-sided thresholding for screening proliferative diabetic retinopathy, Information Technology in Biomedicine, IEEE Transactions on 13 (4) (2009) 528–534.

[22] B. Zhang, L. Zhang, L. Zhang, F. Karray, Retinal vessel extraction by matched filter with first-order derivative of gaussian, Computers in biology and medicine 40 (4) (2010) 438–445.

[23] S. Chaudhuri, S. Chatterjee, N. Katz, M. Nelson, M. Goldbaum, Detection of blood vessels in retinal images using two-dimensional matched filters, IEEE Transactions on medical imaging 8 (3) (1989) 263–269.

[24] A. Hoover, V. Kouznetsova, M. Goldbaum, Locating blood vessels in retinal images by piecewise threshold probing of a matched filter response, Medical Imaging, IEEE Transactions on 19 (3) (2000) 203–210.

[25] A. Can, H. Shen, J. N. Turner, H. L. Tanenbaum, B. Roysam, Rapid automated tracing and feature extraction from retinal fundus images using direct exploratory algorithms, Information Technology in Biomedicine, IEEE Transactions on 3 (2) (1999) 125–138.

[26] O. Chutatape, L. Zheng, S. Krishnan, Retinal blood vessel detection and tracking by matched gaussian and kalman filters, in: Engineering in Medicine and Biology Society, 1998. Proceedings of the 20th Annual International Conference of the IEEE, Vol. 6, IEEE, 1998, pp. 3144–3149.

[27] Y. Sun, Automated identification of vessel contours in coronary arteriograms by an adaptive tracking algorithm, Medical Imaging, IEEE Transactions on 8 (1) (1989) 78–88.

[28] L. Zhou, M. S. Rzeszotarski, L. J. Singerman, J. M. Chokreff, The detection and quantification of retinopathy using digital angiograms, Medical Imaging, IEEE Transactions on 13 (4) (1994) 619–626.

[29] A. F. Frangi, W. J. Niessen, K. L. Vincken, M. A. Viergever, Multiscale vessel enhancement filtering, in: Medical Image Computing and Computer-Assisted InterventationMICCAI98, Springer, 1998, pp. 130–137.

[30] S. R. Aylward, E. Bullitt, Initialization, noise, singularities, and scale in height ridge traversal for tubular object centerline extraction, IEEE transactions on medical imaging 21 (2) (2002) 61–75.

[31] Y. Xu, H. Zhang, H. Li, G. Hu, An improved algorithm for vessel centerline tracking in coronary angiograms, Computer methods and programs in biomedicine 88 (2) (2007) 131–143.

[32] K. K. Delibasis, A. I. Kechriniotis, C. Tsonos, N. Assimakis, Automatic model-based tracing algorithm for vessel segmentation and diameter estimation, Computer methods and programs in biomedicine 100 (2) (2010) 108–122.

[33] B. Nayebifar, H. A. Moghaddam, A novel method for retinal vessel tracking using particle filters, Computers in biology and medicine 43 (5) (2013) 541–548.

[34] Y. Yin, M. Adel, S. Bourennane, Retinal vessel segmentation using a probabilistic tracking method, Pattern Recognition 45 (4) (2012) 1235–1244.

[35] H. Li, J. Zhang, Q. Nie, L. Cheng, A retinal vessel tracking method based on bayesian theory, in: Industrial Electronics and Applications (ICIEA), 2013 8th IEEE Conference on, IEEE, 2013, pp. 232–235.

[36] J. Zhang, H. Li, Q. Nie, L. Cheng, A retinal vessel boundary tracking method based on bayesian theory and multi-scale line detection, Computerized Medical Imaging and Graphics 38 (6) (2014) 517–525.

[37] D. Calvo, M. Ortega, M. G. Penedo, J. Rouco, Automatic detection and characterisation of retinal vessel tree bifurcations and crossovers in eye fundus images, Computer methods and programs in biomedicine 103 (1) (2011) 28–38.

[38] A. Bhuiyan, B. Nath, K. Ramamohanarao, Detection and classification of bifurcation and branch points on retinal vascular network, in: Digital Image Computing Techniques and Applications (DICTA), 2012 International Conference on, IEEE, 2012, pp. 1–8.

[39] D.-M. Baboiu, G. Hamarneh, Vascular bifurcation detection in scale-space, in: Mathematical Methods in Biomedical Image Analysis (MMBIA), 2012 IEEE Workshop on, IEEE, 2012, pp. 41–46.

[40] G. Azzopardi, N. Petkov, Automatic detection of vascular bifurcations in segmented retinal images using

trainable cosfire filters, Pattern Recognition Letters 34 (8) (2013) 922–933.

[41] T. Walter, P. Massin, A. Erginay, R. Ordonez, C. Jeulin, J.-C. Klein, Automatic detection of microaneurysms in color fundus images, Medical image analysis 11 (6) (2007) 555–566.

[42] B. Al-Diri, A. Hunter, D. Steel, M. Habib, T. Hudaib, S. Berry, Review-a reference data set for retinal vessel profiles, in: Engineering in Medicine and Biology Society, 2008. EMBS 2008. 30th Annual International Conference of the IEEE, IEEE, 2008, pp. 2262–2265.

[43] T. Kauppi, V. Kalesnykiene, J.-K. Kamarainen, L. Lensu, I. Sorri, A. Raninen, R. Voutilainen, H. Uusitalo, H. Kälviäinen, J. Pietilä, The diaretdb1 diabetic retinopathy database and evaluation protocol., in: BMVC, 2007, pp. 1–10.